CORONAVIRUS

SARS-CoV-2 Beta variant infection elicits potent lineage-specific and cross-reactive antibodies

S. Momsen Reincke[1,2,3]*†, Meng Yuan[4]†, Hans-Christian Kornau[2,5]†, Victor M. Corman[6,7,8]†, Scott van Hoof[1,2,3], Elisa Sánchez-Sendin[1,2,3], Melanie Ramberger[2,3], Wenli Yu[4], Yuanzi Hua[4], Henry Tien[4], Marie Luisa Schmidt[6,7], Tatjana Schwarz[6,7], Lara Maria Jeworowski[6,7], Sarah E. Brandl[1,2,3], Helle Foverskov Rasmussen[1,2,3], Marie A. Homeyer[1,2,3], Laura Stöffler[1,2,3], Martin Barner[3], Désirée Kunkel[9], Shufan Huo[1], Johannes Horler[1,2,3], Niels von Wardenburg[1,2,3], Inge Kroidl[10,11], Tabea M. Eser[10,11], Andreas Wieser[10,11], Christof Geldmacher[10,11], Michael Hoelscher[10,11], Hannes Gänzer[12], Günter Weiss[13], Dietmar Schmitz[2,5], Christian Drosten[6,7], Harald Prüss[1,2,3]*‡, Ian A. Wilson[4,14]*‡, Jakob Kreye[1,2,3,15]*‡

Severe acute respiratory syndrome coronavirus 2 (SARS-CoV-2) Beta variant of concern (VOC) resists neutralization by major classes of antibodies from COVID-19 patients and vaccinated individuals. In this study, serum of Beta-infected patients revealed reduced cross-neutralization of wild-type virus. From these patients, we isolated Beta-specific and cross-reactive receptor-binding domain (RBD) antibodies. The Beta-specificity results from recruitment of VOC-specific clonotypes and accommodation of mutations present in Beta and Omicron into a major antibody class that is normally sensitive to these mutations. The Beta-elicited cross-reactive antibodies share genetic and structural features with wild type–elicited antibodies, including a public VH1-58 clonotype that targets the RBD ridge. These findings advance our understanding of the antibody response to SARS-CoV-2 shaped by antigenic drift, with implications for design of next-generation vaccines and therapeutics.

In the course of the COVID-19 pandemic, multiple severe acute respiratory syndrome coronavirus 2 (SARS-CoV-2) lineages have emerged, including lineages defined as variants of concern (VOCs), such as Alpha (also known as lineage B.1.1.7), Beta (B.1.351), Gamma (P.1), Delta (B.1.617.2), and recently, Omicron (B.1.1.529). VOCs are associated with increased transmissibility, virulence, or resistance to neutralization by sera from vaccinated and convalescent individuals who were infected with the original strain (*1*–*7*). These distinct lineages carry a variety of mutations in the spike protein, several of which are within the receptor-binding domain (RBD), especially at residues K417, L452, T478, E484, and N501. Some mutations such as N501Y are associated with enhanced binding to angiotensin-converting enzyme 2 (ACE2), largely driving the global spread of VOCs that incorporate these mutations (*2*). (Single-letter abbreviations for the amino acid residues are as follows: A, Ala; C, Cys; D, Asp; E, Glu; F, Phe; G, Gly; H, His; I, Ile; K, Lys; L, Leu; M, Met; N, Asn; P, Pro; Q, Gln; R, Arg; S, Ser; T, Thr; V, Val; W, Trp; and Y, Tyr. In the mutants, other amino acids were substituted at certain locations; for example, N501Y indicates that asparagine at position 501 was replaced by tyrosine.)

However, with increasing immunity either through natural infection or vaccination, antibody escape will become more relevant in emerging VOCs. Many studies have investigated RBD antibodies in COVID-19 patients before identification of SARS-CoV-2 variants, and we refer to these as wild-type antibodies. Wild-type RBD antibodies revealed a preferential response toward distinct epitopes, with enriched recruitment of particular antibody germline genes, where the most prominent were VH3-53 and closely related VH3-66, as well as VH1-2 (*8*, *9*). Structural and functional classification of wild-type RBD monoclonal antibodies (mAbs) has demonstrated that mAbs from these three enriched germline genes form two major classes of receptor-binding site (RBS) mAbs whose binding and neutralizing activity depends on either K417 or E484 (*9*, *10*). Mutations at these key residues (K417N and E484K) together with N501Y are hallmarks of Beta (*2*) and largely account for the reduced neutralizing activity of sera from vaccinated and convalescent individuals against this VOC (*1*–*6*, *11*, *12*). Of the first four VOCs (Alpha through Delta), Beta shows the highest resistance to neutralization by wild-type–elicited sera (*12*), suggesting conspicuous differences in its antigenicity (*13*). First reports indicate that Omicron, which shares K417N and N501Y with Beta and carries a different mutation at the third key residue (E484A) as well as 34 further spike mutations, shows even higher resistance to neutralization by wild-type–elicited sera (*14*). Although mutations at position K417 and E484 influence the antigenicity of the RBD, little is known about the antibody response elicited by Beta infection. For example, it is unknown whether antibodies targeting the RBD Beta share the preferential recruitment of particular germline genes with wild-type antibodies, or whether VOC-defining mutations K417N and E484K could be accommodated in the canonical binding modes of public VH3-53/VH3-66 antibody classes. Thus, we set out to explore genetic, functional, and structural features of the antibody response against RBD in Beta-infected individuals.

We identified 40 individuals infected with SARS-CoV-2 Beta from three metropolitan areas in Germany and Austria (table S1) and collected serum at 38.6 ± 19.2 days after their first positive SARS-CoV-2 reverse transcription polymerase chain reaction (RT-PCR) test. The patients' immunoglobulin G (IgG) bound to wild-type nucleocapsid protein, wild-type spike, or both proteins in 37 of 40 patients, and with stronger reactivity to RBD Beta than to wild-type RBD (fig. S1A). The patients' sera also inhibited ACE2 binding to RBD Beta to a greater extent than to wild-type RBD (fig. S1B and table S1). Reactivity to wild-type spike S1 was confirmed in an additional commercially available enzyme-linked immunosorbent assay (ELISA); however, only 23 of 40 samples tested positive, according to the manufacturer's cutoff (fig. S1, C and D). In a plaque reduction neutralization test (PRNT), 37 of 40 sera neutralized an authentic SARS-CoV-2 Beta isolate with a half-maximal inhibitory concentration (IC_{50}) at 1:20 dilution or greater (Fig. 1A). By contrast, only 11 of 40 sera neutralized wild-type virus (Fig. 1B). The neutralizing activity against the two isolates was modestly correlated (fig. S1E), with a ~20-fold reduction of neutralizing activity against wild-type virus compared with Beta (Fig. 1C and fig. S1F). A converse effect has been reported after

Downloaded from https://www.science.org at Deutsches Zentrum fr Neurodegenerative Erkrankungen on June 14, 2022

[1]Department of Neurology and Experimental Neurology, Charité–Universitätsmedizin Berlin, corporate member of Freie Universität Berlin and Humboldt-Universität zu Berlin, Berlin, Germany. [2]German Center for Neurodegenerative Diseases (DZNE) Berlin, Berlin, Germany. [3]Helmholtz Innovation Lab BaoBab (Brain Antibody-omics and B-cell Lab), Berlin, Germany. [4]Department of Integrative Structural and Computational Biology, The Scripps Research Institute, La Jolla, CA 92037, USA. [5]Neuroscience Research Center (NWFZ), Cluster NeuroCure, Charité–Universitätsmedizin Berlin, corporate member of Freie Universität Berlin and Humboldt-Universität zu Berlin, Berlin, Germany. [6]Institute of Virology, Charité–Universitätsmedizin Berlin, corporate member of Freie Universität Berlin and Humboldt-Universität zu Berlin, Berlin, Germany. [7]German Centre for Infection Research (DZIF), Berlin, Germany. [8]Labor Berlin–Charité Vivantes GmbH, Berlin. [9]Flow and Mass Cytometry Core Facility, Berlin Institute of Health at Charité–Universitätsmedizin Berlin, Berlin, Germany. [10]Division of Infectious Diseases and Tropical Medicine, Medical Center of the University of Munich (LMU), Germany. [11]German Center for Infection Research (DZIF), partner site Munich, Germany. [12]Department of Internal Medicine, BKH Schwaz, Schwaz, Austria. [13]Department of Internal Medicine II, Medical University of Innsbruck, Innsbruck, Austria. [14]The Skaggs Institute for Chemical Biology, The Scripps Research Institute, La Jolla, CA 92037, USA. [15]Department of Pediatric Neurology, Charité–Universitätsmedizin Berlin, corporate member of Freie Universität Berlin and Humboldt-Universität zu Berlin, Berlin, Germany.
*Corresponding author. Email: momsen.reincke@charite.de (S.M.R.); harald.pruess@charite.de (H.P.); wilson@scripps.edu (I.A.W.); jakob.kreye@charite.de (J.K.)
†These authors contributed equally to this work.
‡These authors contributed equally to this work.

immune responses against wild-type RBD in convalescent and vaccinated individuals (*2*), in which neutralization of SARS-CoV-2 Beta was ~8- to ~14-fold reduced compared with wild-type virus (*1*–*6*). No positive correlation was found between neutralizing antibodies against Beta and the time point of sample collection relative to first positive PCR test (fig. S1G). Neutralizing antibodies against Beta modestly correlated with age (fig. S1H), but no statistically significant gender difference was observed (fig. S1I). Collectively, these data show that sera from Beta-infected patients exhibit reduced cross-reactivity to wild-type SARS-CoV-2, therefore affecting diagnostic antibody testing when using wild-type antigens and adding complexity to the concept of defining a threshold for protective antibody titers.

To investigate the effect of this difference in reactivity between RBD Beta and wild-type RBD at the level of mAbs elicited by SARS-CoV-2 Beta infection, we isolated $CD19^{+}CD27^{+}$ memory B cells from the peripheral blood of 12 donors in our cohort by means of fluorescence activated cell sorting using a recombinant RBD Beta probe (fig. S2, A and B). Using single-cell Ig gene sequencing (*15*, *16*), we derived 289 pairs of functional heavy (IGH) and light (IGL) chain sequences from IgG mAbs (table S2). Sequence analysis showed enrichment of certain genes compared with mAbs derived from healthy, noninfected individuals—including VH1-58, VH3-30, VH4-39, and VH3-53—illustrating a preferential recruitment of certain VH genes (Fig. 2A), VH-JH gene combinations (fig. S3A), and variable light chain genes (fig. S3B). For some genes such as VH1-58 and VH3-53, enrichment has previously been identified in CoV-AbDab, a database of published SARS-CoV-2 mAbs (*9*, *17*). We confirmed this finding for all human wild-type RBD mAbs in CoV-AbDab (Fig. 2A). Consistent with reports from wild-type SARS-CoV-2 infections (*18*–*20*), the somatic hypermutation (SHM) count was generally low in mAbs of our cohort (fig. S3C). Together, these findings argue for conservation of certain antibody sequence features between antibody responses in different donors and between antibody responses elicited against Beta and wild-type virus. Hence, we compared antibody sequences after Beta infection with all previously published wild-type RBD mAbs and identified several clonotypes shared between both datasets (Fig. 2B), some of which were present in multiple patients of our study (Fig. 2C). Thus, a subset of the antibodies to RBD Beta and wild-type RBD converge upon recruitment of specific germline genes.

However, other gene enrichments found in our study, such as VH4-39, have not been identified within the CoV-AbDab mAbs (Fig. 2A) (*9*), exemplifying concurrent divergence in the antibody response to the different RBDs. VH1-2, one of the most common genes contributing to the RBD antibody response to wild-type SARS-CoV-2, was strongly reduced in our dataset (Fig. 2A and table S2), which is consistent with the dependence of VH1-2 mAbs on E484 (*9*). VH3-53/VH3-66 antibodies bind to wild-type RBD in two canonical binding modes, which involve residues K417 and E484, respectively; binding and neutralization of these antibodies are strongly affected by the K417N and E484K mutations in RBD Beta (*9*, *21*). We therefore hypothesized a similarly reduced recruitment of VH3-53/VH3-66 mAbs after Beta infection. Unexpectedly, we identified 15 VH3-53/VH3-66 mAbs, albeit at a reduced frequency compared with that of the CoV-AbDab dataset (4.7 versus 19.4%), but still at an increased frequency compared with that of healthy donors (Fig. 2A), thus indicating either a noncanonical binding mode or accommodation of these mutations into the known binding modes.

To determine the binding properties of antibodies elicited by SARS-CoV-2 Beta, we selected representative mAbs for expression (table S2). We identified 81 mAbs with strong binding to RBD Beta (table S3). Of those, 44 revealed comparable binding to wild-type RBD and were considered cross-reactive mAbs, whereas 37 mAbs did not bind wild-type RBD and were considered Beta-specific. There were no differences in V gene SHMs, CDR H3/L3 hydrophobicity, and ACE2-binding inhibition between Beta-specific and cross-reactive antibodies (fig. S4, A to C), but the cross-reactive antibodies had a slightly shorter CDR H3/L3 and lower isoelectric point of their CDR H3 (fig. S4, D and E). The neutralization potencies were similar between Beta-specific and cross-reactive mAbs (fig. S4F). All Beta-specific VH3-30 mAbs paired with JH6 (fig. S4G), whereas all cross-reactive VH3-30 mAbs paired with JH4 (fig. S4H). Competition experiments showed that many of the strongly neutralizing Beta-elicited mAbs compete for RBD binding (fig. S4I), indicating that they target similar epitopes.

Next, we aimed to determine the residues that define the binding selectivity for the 37 RBD Beta-specific mAbs and performed ELISAs with single-mutant constructs of RBD Beta and wild-type RBD. For all three Beta-defining RBD mutations (K417N, E484K, and N501Y), we identified mAbs with RBD binding that depended on a single residue. The Beta-specificity of the other mAbs was dependent on multiple residues (Fig. 3A). RBD Beta–specific mAbs were encoded by diverse VH genes (Fig. 3A and table S2), and 26 of the RBD Beta-specific mAbs (70.3%) neutralized the authentic SARS-CoV-2 Beta isolate (Fig. 3A). All nine Beta-specific VH4-39 mAbs from three different patients were Y501-dependent, comprising 81.8% of all Y501-dependent mAbs. This finding suggests a common binding mode of these clonally unrelated mAbs that depends on Y501—which is a residue present in RBD Beta, Alpha, Gamma, and Omicron but not Delta—and may explain the frequent use of VH4-39 in mAbs to RBD Beta (Fig. 2A). VH4-39 Y501–dependent mAbs revealed few SHMs in VH genes but no uniform pattern in other sequence features (fig. S5A). Although all VH4-39 RBD Beta-specific mAbs bind to a Y501-dependent epitope, their neutralization activity showed noticeable differences (IC_{50} ranging from 5.2 to 947 ng/ml) (fig. S5B). Surface plasmon resonance measurements of these mAbs to RBD Beta revealed equilibrium dissociation constants (K_D) between 3.39 and 80.4 nM (fig. S5C) with correlation to their PRNT-derived

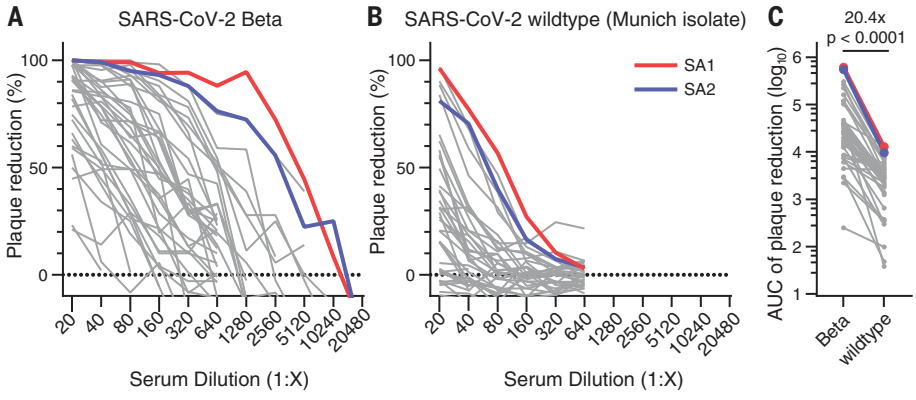

Fig. 1. Authentic virus neutralization of sera from individuals after infection with SARS-CoV-2 Beta. (**A** and **B**) Neutralizing activity of sera of patients infected with SARS-CoV-2 Beta variant was measured by using a plaque-reduction neutralization assay with the indicated authentic virus. Results are given as reduction of plaque number at indicated serum dilutions. Patients SA1 and SA2 mounted the strongest antibody response, which are highlighted in red and blue, respectively. Means of duplicate measurements are shown. Values below zero indicate no plaque reduction. (**C**) Change in neutralization activity against SARS-CoV-2 Beta and wild-type SARS-CoV-2 based on area-under-the-curve (AUC) calculations from authentic virus PRNT curves [shown in (A) and (B)]. Mean fold change is indicated above the *P* value. Statistical analysis was performed by using a Wilcoxon matched-pairs signed-rank test with two-tailed *P* value.

Downloaded from https://www.science.org at Deutsches Zentrum fr Neurodegenerative Erkrankungen on June 14, 2022

IC_{50} values (fig. S5D), providing an explanation for the variability in neutralizing activity within VH4-39 Y501-dependent mAbs.

Furthermore, we identified three VH3-53/VH3-66 mAbs with RBD Beta specificity that all showed neutralizing activity. To determine whether this RBD Beta specificity results from a noncanonical binding mode or accommodation of Beta-defining mutations in one of the two main VH3-53/VH3-66 mAb binding modes, we determined a crystal structure of VH3-53 antibody CS23 in complex with RBD Beta. VH3-53/VH3-66 mAbs with short CDRs H3 (<15 amino acids) target the RBS of wild-type RBD through a canonical mode (*10*, *22*–*25*) that is highly sensitive to the K417N mutation (*9*). CS23 contains a CDR H3 with only 10 amino acids and is specific to N417 RBDs, including RBD Beta (Fig. 3A). However, CS23 binds to RBD Beta in the canonical mode, with a nearly identical approach angle compared with that of a representative wild-type VH3-53 antibody CC12.3 (Fig. 3B) (*24*). We previously showed that the CDR H1 ^{33}NY^{34} and H2 ^{53}SGGS^{56} motifs of VH3-53/VH3-66 mAbs are critical for RBD recognition (*24*). We found that CS23 retains these motifs and that they interact with the RBD in the same way (Fig. 3, C and D). Residues in CDR H3 usually interact with K417 and thus confer specificity to the wild-type RBD (*9*). For example, variable region of immunoglobulin heavy chain (V_H) D97 of CC12.1 forms a salt bridge with the outward-facing RBD-K417, whereas V_H F99 and V_H G97 of CC12.3 interact with K417 through cation-π and hydrogen bonds (H-bonds), respectively (Fig. 3, E and F). Instead, in RBD Beta, the shorter N417 flips inward and H-bonds with RBD-E406 and Q409 (Fig. 4G). V_H M98 occupies the vacated space and interacts with RBD-Y453, L455, and variable region of immunoglobulin light chain (V_L) W91 in a hydrophobic pocket. Modeling shows that K417 would be unfavorable for RBD binding to CS23 (fig. S6A). CDR H3 contains a V_H ^{96}TAMA^{99} sequence that forms an ST motif that stabilizes CDR H3 and the orientation of M98. The first serine (S) or threonine (T) residue in a four- or five-residue ST motif makes two internal H-bonds from the side-chain oxygen of residue *i* to the main-chain NH of residue *i* + 2 or *i* + 3, and between the main-chain oxygen of residue *i* and the main-chain NH of residue *i* + 3 or *i* + 4. In this case, the T96 side-chain H-bonds with the main-chain NH of M98, and the T96 main-chain oxygen H-bonds with the main-chain NH of A99 (fig. S6A).

This V_H ^{96}TxMx^{99} motif is different from all known CDR H3 of VH3-53/VH3-66 antibodies to RBD (*17*) and explains the newly acquired specificity of this VH3-53 antibody for an RBD with N417. Previously, wild-type VH3-53 antibody COVOX-222 was shown to cross-react with RBD Beta despite interacting with K417 and N501, but nevertheless binds the RBD in the canonical mode; in this case, a rare SHM V_L S30P mutation accommodated Y501 (fig. S6, B and C) (*1*). Likewise, for CS23, the CDR L1 ^{30}SK^{31} dipeptide is mutated to ^{30}GQ^{31} and accommodates Y501 in Beta (fig. S6D). Another VH3-53 antibody from our cohort, CS82, is highly cross-reactive and binds SARS-CoV (Fig. 4A), which was not known for any previous VH3-53 antibodies. CS82 competes with CR3022, which binds to a lateral face of the RBD outside the RBS (fig. S6E) and might suggest a possible alternative binding mode or orientation compared with the two previously identified binding modes of wild-type VH3-53 antibodies that are usually sensitive either to K417N or to E484K (*23*, *24*). Collectively, VH3-53/VH3-66 mAbs contribute to the immune response to RBD Beta with mAbs that accommodate Beta-specific mutations in canonical modes and by mAbs that may bind in alternative binding modes.

We next aimed to characterize the functional breadth of the cross-reactive mAbs. Twenty of the 44 cross-reactive mAbs (45.5%) neutralized authentic SARS-CoV-2 Beta isolate (Fig. 4A). To investigate their cross-reactivity against further RBD variants, we performed ELISAs with RBD

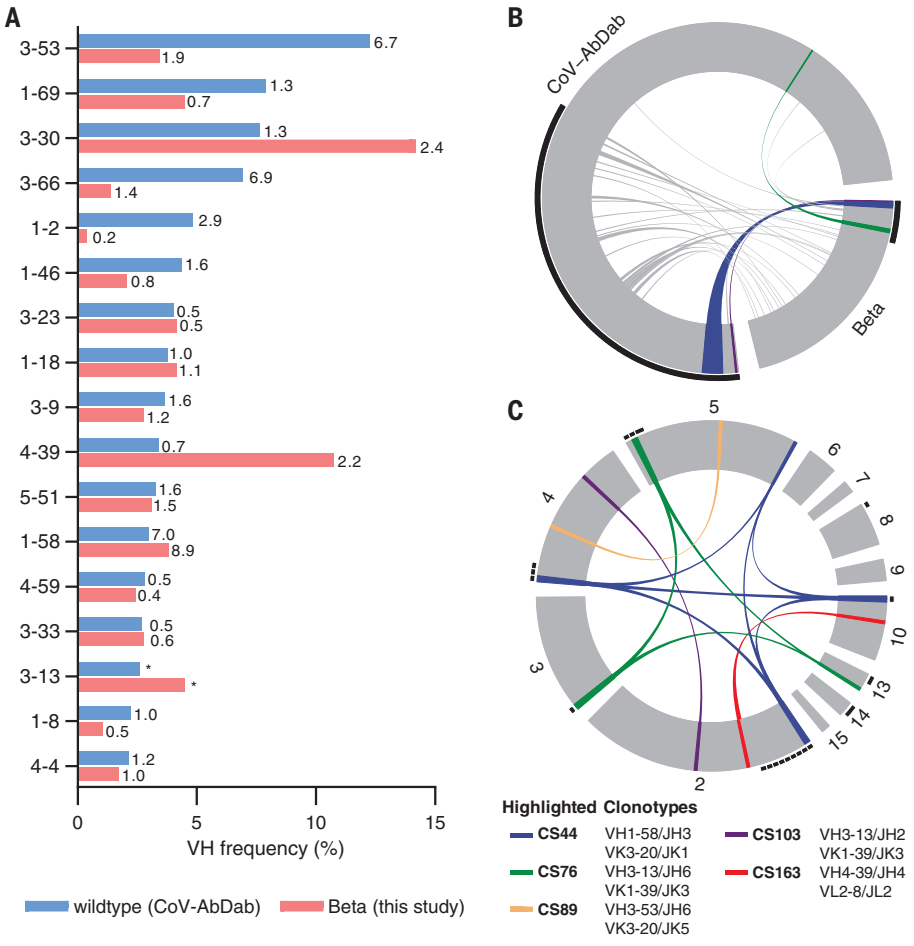

Fig. 2. Germline gene usage and clonotype analysis of Beta-elicited antibodies. (**A**) VH gene usage of 289 RBD Beta IgG mAbs from this study (red) is compared with 1037 wild-type RBD mAbs from 96 previously published studies (blue, CoV-AbDab) (*17*). Frequencies of mAbs encoded by each VH gene are shown as bars. Enrichment of indicated VH genes is compared with that of healthy individuals (*31*), with fold-enrichment shown as number next to bars. VH gene frequencies that were not reported in healthy individuals (*31*) are indicated with an asterisk. Only VH genes with a frequency of at least 2% in CoV-AbDab are shown, and VH genes are ordered by frequency in CoV-AbDab. (**B**) Circos plot shows the relationship between 289 IgG mAbs from this study (Beta) and 1037 previously published human mAbs reactive to wild-type RBD (CoV-AbDab) from 96 studies (*17*). Interconnecting lines display clonotypes shared between both datasets, as defined by the usage of the same V and J gene on both Ig heavy and light chain. Thin black lines at the outer circle border indicate expanded clonotypes within the respective data set. (**C**) Circos plot displaying the 289 IgG mAbs from this study grouped per patient. Interconnecting colored lines indicate clonotypes found in more than one patient. Small black at the outer circle border indicate clonally expanded clones within one patient. In (B) and (C), colored interconnecting lines depict clonotypes found in more than one patient of our cohort.

Downloaded from https://www.science.org at Deutsches Zentrum fr Neurodegenerative Erkrankungen on June 14, 2022

constructs of VOCs Alpha through Delta and SARS-CoV. Whereas only two mAbs (10%) strongly detected SARS-CoV RBD, the majority of cross-reactive antibodies bound the RBD of Alpha, Gamma, and Delta (Fig. 4A). In PRNT assays with further authentic virus isolates, 15 (75%) Beta-neutralizing cross-reactive mAbs also neutralized wild-type virus, and 14 (70%) neutralized a Delta virus isolate, which of the VOCs was the most antigenically distinct from the others at the time of testing (Fig. 4A). Six cross-neutralizing antibodies were encoded by VH1-58 (Fig. 4A). VH1-58 is the most enriched germline VH gene in RBD antibodies in both Beta and wild-type infection (Fig. 2A) (*26*). VH1-58 RBD antibodies almost exclusively pair with JH3 (fig. S3A). This VH1-58/JH3/VK3-20/JK1 clonotype has been described in individuals infected with wild-type virus (*20*, *26*) and found in several patients within our cohort (Fig. 2C and table S6), representing 2.4% of all Beta-elicited IgG mAbs analyzed in this study (table S2).

To elucidate the structural basis of this public broadly reactive clonotype, we determined crystal structures of CS44 and CV07-287, a mAb of the same clonotype that was isolated from a wild-type–infected individual (*19*), in complex with RBD Beta and wild-type RBD, respectively (Fig. 4B). We compared the structures of CS44 and CV07-287 with other published VH1-58 antibodies including COVOX-253 (*27*), S2E12 (*28*), A23-58.1, and B1-182.1 (*26*). These antibodies all target the RBD in the same binding mode (Fig. 4B), which suggests that this public clonotype is structurally conserved. The dominant interaction of VH1-58 antibodies is with the RBD ridge region (residues 471 to 491), which accounts for ~75% of the entire epitope surface. Most of the VOC mutations occur outside of the ridge region (for example, residues 417, 452, and 501) and are distant from the binding sites of VH1-58 antibodies CV07-287 and CS44 (Fig. 4, C and D). T478 interacts with VH1-58 antibodies, but mutation to a lysine can be accommodated (Fig. 4A) (*26*). V_H W50 and Y52 in CDR H2 provide hydrophobic interactions with the RBD (Fig. 4, E and F). CDR H3 also forms extensive interactions with the RBD (Fig. 4, G and H). The CDR H3 sequences of 38 antibodies that belong to this clonotype (Fig. 4I) (*17*) are highly conserved, and all contain a disulfide bond between V_H C97 and C100b, with four relatively small residues (G, S, and T) in between (Fig. 4, I, G, and H). V_H D100d is also conserved (Fig. 4I), forming H-bonds with S477 and T478 (Fig. 4, G and H). In addition, the conserved V_H P95 and F100f (Fig. 4I) stack with RBD-F486 together with V_H W50, V_L Y91, and V_L W96 (Fig. 4, G and H). Although E484 is often an important residue for antibody binding on the ridge region, here it is 5 Å distant from the antibodies, and mutations at this site have not

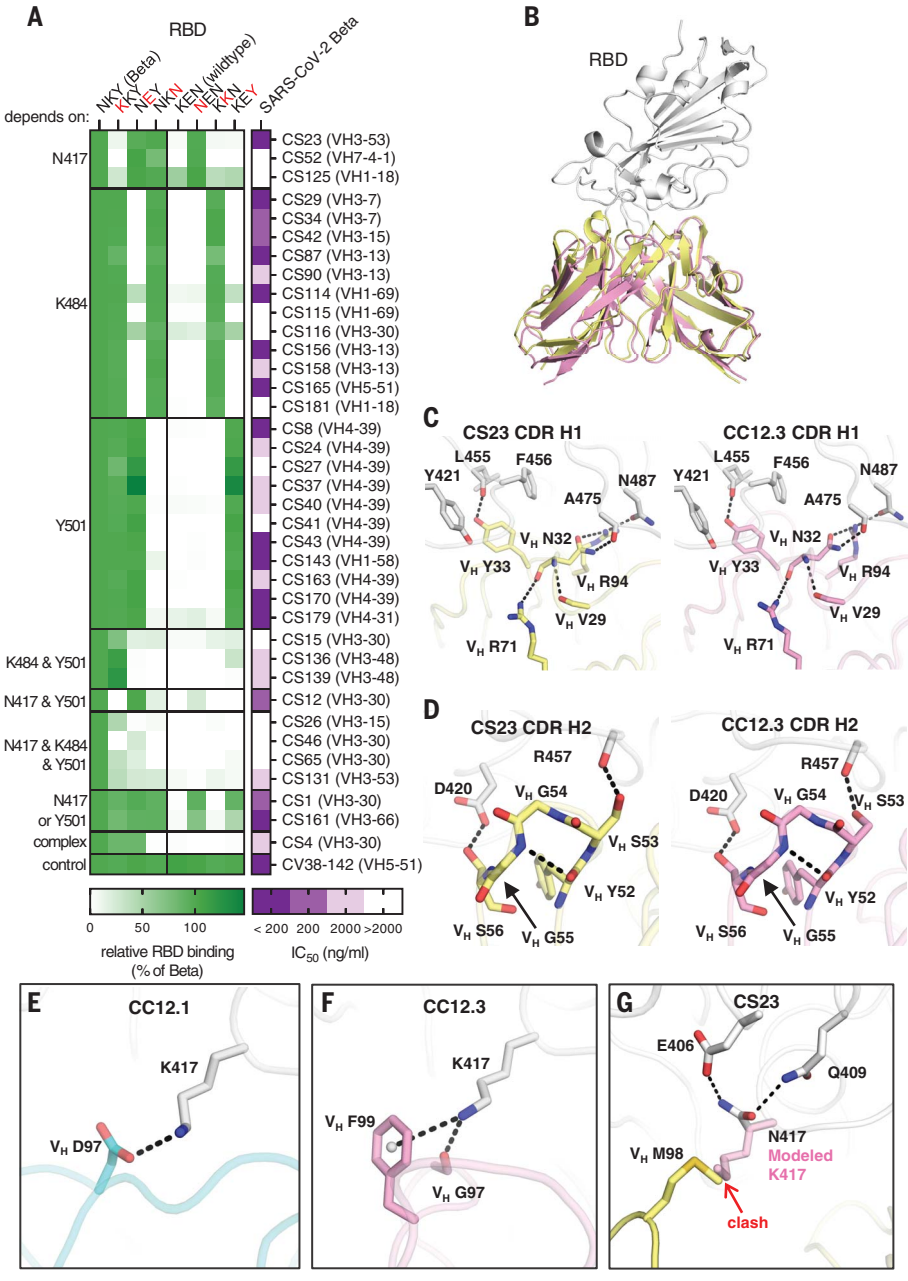

Fig. 3. Binding, neutralization, and structures of Beta-specific antibodies. (**A**) Neutralization of indicated Beta-specific mAbs against authentic Beta virus is shown in purple. Binding to single-point mutant RBD constructs with the indicated amino-acid residues at positions 417, 484, and 501 is shown in green, normalized to RBD Beta. (**B** to **G**) Structural comparison of VH3-53 mAbs between Beta-specific CS23 and wild-type–specific CC12.1 and CC12.3. (B) CC12.3 and CS23 adopt the same binding mode. The crystal structure of CC12.3 (pink) in complex with wild-type RBD was superimposed onto CS23 (yellow) in complex with RBD Beta. Only the variable domains of the antibodies are shown for clarity. A small local conformational difference was observed between CS23-bound RBD Beta and CC12.3-bound wild-type RBD (191 Cα, root mean square deviation = 0.8 Å). [(C) and (D)] Comparison of the (C) CDR H1 ("NY" motif) and (D) CDR H2 ("SGGS" motif) between CS23 and CC12.3. [(E) to (G)] Structures of CDR H3 of (E) CC12.1, (F) CC12.3, and (G) CS23. A modeled side chain of K417 is shown as transparent pink sticks, which would be unfavorable for binding to CS23, where V_H M98 occupies this pocket. Structures of CC12.1 (PDB 6XC3, cyan), CC12.3 (PDB 6XC4, pink), and CS23 (this study, yellow) are used throughout this figure, and the RBD is shown in white. Hydrogen bonds, salt bridges, or cation-π bonds are represented with black dashed lines.

Downloaded from https://www.science.org at Deutsches Zentrum fr Neurodegenerative Erkrankungen on June 14, 2022

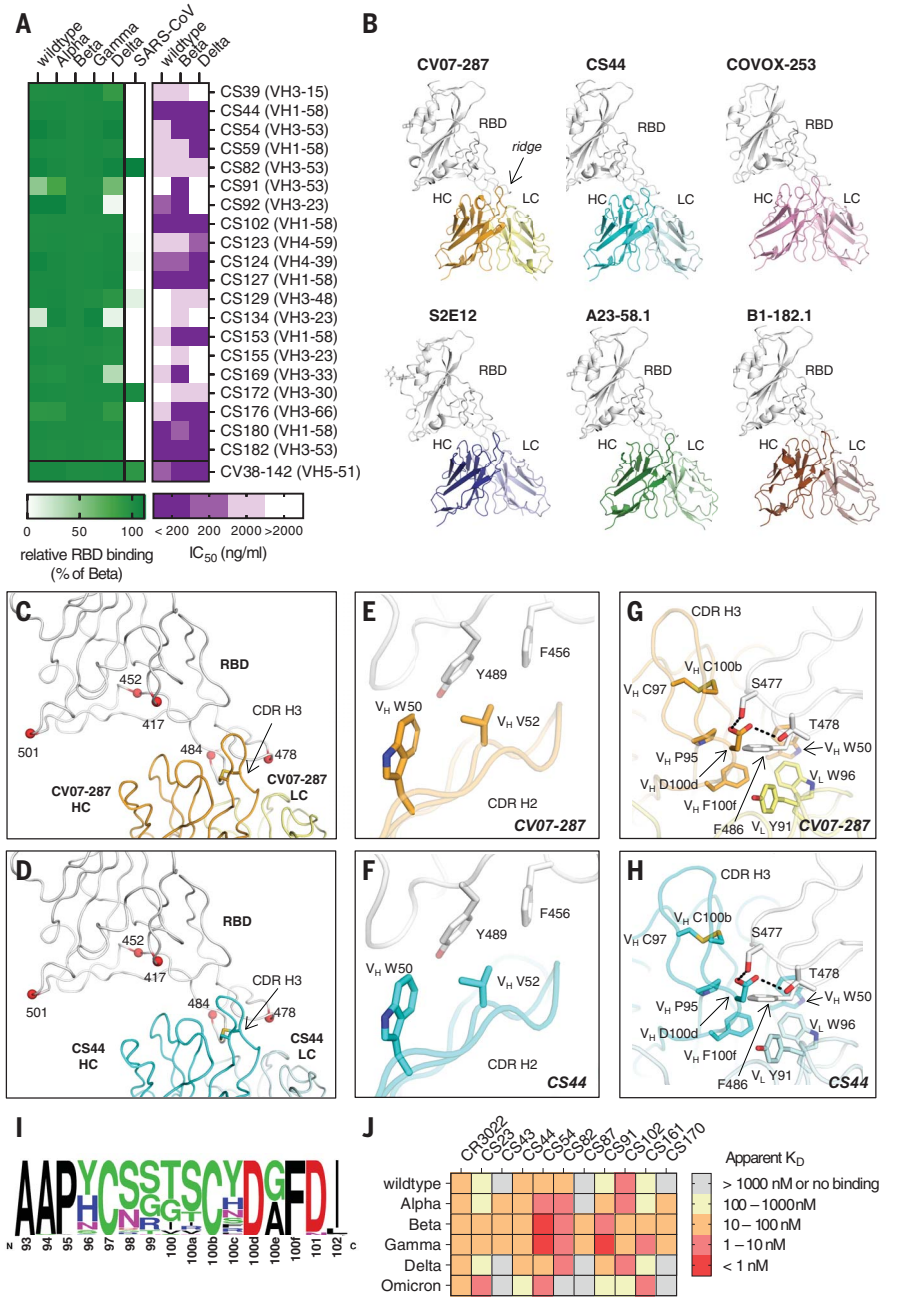

Fig. 4. Characterization of cross-reactive mAbs and crystal structures of CV07-287 and CS44. (**A**) Neutralization of cross-reactive antibodies against authentic Beta, Delta, and wild-type virus is shown in purple. Binding to the indicated RBD constructs is shown in green, normalized to RBD Beta. (**B**) VH1-58 antibodies target SARS-CoV-2 RBD through the same binding mode. Crystal structures of CV07-287 in complex with wild-type RBD and CS44 in complex with RBD Beta are shown. COVA1-16 Fab that was used in the crystallization to form the crystal lattice is not shown for clarity. Structures of VH1-58 antibodies from other studies are shown for comparison, including COVOX-253 (PDB 7BEN), S2E12 (PDB 7K45), A23-58.1 (PDB 7LRT), and B1-182.1 (PDB 7MM0). All structures are shown in the same orientation, with the constant domains of the Fab omitted for clarity. The location of the ridge region of the RBD is indicated at top right. (**C** and **D**) Mutated residues in VOCs B.1.1.7 (Alpha), B.1.351 (Beta), B.1.617.2 (Delta), and P.1 (Gamma) variants are represented by red spheres. All of these residues are distant from VH1-58 antibodies (C) CV07-287 and (D) CS44, except for T478. The disulfide bond in each CDR H3 is shown as sticks. (**E** to **H**) Detailed interactions between the RBD and [(E) and (G)] CV07-287 and [(F) and (H)] CS44, respectively. RBDs are shown in white, with heavy and light chains of CV07-287 in orange and yellow, and those of CS44 in cyan and light cyan, respectively. Interactions of CDR H2 are shown in (E) and (F), and those of CDR H3 are in (G) and (H). Hydrogen bonds are represented with black dashed lines. (**I**) Sequence logo of CDR H3 of VH1-58/VK3-20 antibodies. CDR H3 sequences of VH1-58/VK3-20 antibodies from COVID-19 patients (*17*) were aligned and analyzed with WebLogo. (**J**) Affinity of indicated Beta-elicited mAbs to RBD of indicated VOCs was determined by means of biolayer interferometry.

been reported as being sensitive for VH1-58 antibodies.

Thousands of anti-SARS-CoV-2 mAbs were isolated before the VOCs started to emerge (*17*), many of which are highly potent but with varying sensitivity to VOCs. We characterized the antibody response to the RBD after SARS-CoV-2 Beta infection to provide insights into diverging and converging features of antibodies elicited by this lineage compared with wild-type–elicited antibodies. Recently, the highly mutated Omicron variant has further increased the complexity of SARS-CoV-2 cross-variant immunity and resembles Beta as an antigenically distant VOC. On the basis of their shared RBD mutations, we hypothesized that some Beta-elicited mAbs also bind Omicron. Accordingly, VH3-53 mAb CS23, which binds the shared mutated residues N417 and Y501, showed comparable binding to Omicron and Beta (Fig. 4J). By contrast, Y501-dependent VH4-39 antibodies CS43 and CS170 did not bind to Omicron, suggesting that other mutations in Omicron impede binding of this clonotype. Similarly, VH1-58 mAbs CS44 and CS102 also showed a drastic reduction in affinity to Omicron (Fig. 4J), suggesting that Omicron may not be efficiently neutralized by this public clonotype that exhibits ultrahigh potency and high resistance to VOCs Alpha, Beta, Gamma, and Delta (*26*). These findings emphasize the antigenic complexity and high temporal dynamics that define antibody immunity against SARS-CoV-2 in the context of ongoing antigenic drift and provide insights for next-generation vaccine design and antibody therapeutics. For example, simultaneous or sequential immunization with vaccines based on diverse RBD sequences could be evaluated for superiority in induction of cross-variant immunity. Although large-scale production of novel vaccine candidates based on the Omicron sequence have been initiated, those based on the Beta sequence already show promising cross-variant antibody titers in preclinical

Downloaded from https://www.science.org at Deutsches Zentrum fr Neurodegenerative Erkrankungen on June 14, 2022

studies (*29*, *30*), which led to the subsequent initiation of a phase II/III clinical trial. These clinical trials should be complemented by studies of the immune response against recent and future SARS-CoV-2 variants, including Delta and Omicron, which are currently dominating global infections.

REFERENCES AND NOTES

1. W. Dejnirattisai *et al*., *Cell* **184**, 2939–2954.e9 (2021).
2. P. Wang *et al*., *Nature* **593**, 130–135 (2021).
3. M. Hoffmann *et al*., *Cell* **184**, 2384–2393.e12 (2021).
4. M. Hoffmann *et al*., *Cell Rep.* **36**, 109415 (2021).
5. D. Planas *et al*., *Nat. Med.* **27**, 917–924 (2021).
6. D. Zhou *et al*., *Cell* **184**, 2348–2361.e6 (2021).
7. M. Widera *et al*., *J. Infect. Dis.* **224**, 1109–1114 (2021).
8. M. Rapp *et al*., *Cell Rep.* **35**, 108950 (2021).
9. M. Yuan *et al*., *Science* **373**, 818–823 (2021).
10. C. O. Barnes *et al*., *Nature* **588**, 682–687 (2020).
11. D. Geers *et al*., *Sci. Immunol.* **6**, eabj1750 (2021).
12. C. Lucas *et al*., *Nature* **600**, 523–529 (2021).
13. M. Cevik, N. D. Grubaugh, A. Iwasaki, P. Openshaw, *Cell* **184**, 5077–5081 (2021).
14. E. Cameroni *et al*., *Nature* 10.1038/s41586-021-04386-2 (2021).
15. J. Kreye *et al*., *Brain* **139**, 2641–2652 (2016).
16. T. Tiller *et al*., *J. Immunol. Methods* **329**, 112–124 (2008).
17. M. I. J. Raybould, A. Kovaltsuk, C. Marks, C. M. Deane, *Bioinformatics* **37**, 734–735 (2021).
18. C. Kreer *et al*., *Cell* **182**, 1663–1673 (2020).
19. J. Kreye *et al*., *Cell* **183**, 1058–1069.e19 (2020).
20. D. F. Robbiani *et al*., *Nature* **584**, 437–442 (2020).
21. Z. Wang *et al*., *Nature* **592**, 616–622 (2021).
22. C. O. Barnes *et al*., *Cell* **182**, 828–842.e16 (2020).
23. N. C. Wu *et al*., *Cell Rep.* **33**, 108274 (2020).
24. M. Yuan *et al*., *Science* **369**, 1119–1123 (2020).
25. M. Yuan, H. Liu, N. C. Wu, I. A. Wilson, *Biochem. Biophys. Res. Commun.* **538**, 192–203 (2021).
26. L. Wang *et al*., *Science* **373**, eabh1766 (2021).
27. W. Dejnirattisai *et al*., *Cell* **184**, 2183–2200.e22 (2021).
28. M. A. Tortorici *et al*., *Science* **370**, 950–957 (2020).
29. A. J. Spencer *et al*., *bioRxiv* 447308 [Preprint] (2021).
30. B. Ying *et al*., *Sci. Transl. Med.* 10.1126/scitranslmed.abm3302 (2021).
31. S. D. Boyd *et al*., *J. Immunol.* **184**, 6986–6992 (2010).

ACKNOWLEDGMENTS

We thank all study participants who devoted samples and time to our research; K. Stahlberg and M. Zuo for patient recruitment; S. Bandura, M. Sillmann, D. Brandl, P. Tscheak, and S. Engl for excellent technical assistance; and M. A. Müller and D. Niemeyer for support with BSL3 work. We acknowledge BIAFFIN GmbH & Co. KG (Kassel, Germany) for performance of SPR measurements and the Flow and Mass Cytometry Core Facility at Charité–Universitätsmedizin Berlin for support with single-cell sorting. We thank R. Stanfield for assistance in data collection, F. Zhao for assistance in the biolayer interferometry binding assay, and the staff of Advanced Light Source beamline 5.0.1 and Stanford Synchrotron Radiation Laboratory (SSRL) beamline 12-1 for assistance. SARS-CoV-2 RBD variants antigens for sera testing were kindly provided by InVivo BioTech Services GmbH (Hennigsdorf, Germany) to the Seramun Diagnostica GmbH (Heidesee, Germany). S.M.R. and J.K. are participants in the BIH-Charité Junior Clinician Scientist Program, and V.M.C is supported by Berlin Institute of Health (BIH) Charité Clinician Scientist program, both funded by Charité–Universitätsmedizin Berlin and the Berlin Institute of Health. **Funding:** This work was supported by the Bill and Melinda Gates Foundation INV-004923 (I.A.W.); the Bavarian State Ministry of Science and the Arts; University Hospital; Ludwig-Maximilians-Universität Munich; German Ministry for Education and Research (project 01KI20271, M.H.; Connect-Generate 01GM1908D, H.P.); the Helmholtz Association (ExNet-0009-Phase2-3, D.S.; HIL-A03, H.P.); the German Research Foundation (DFG) (FOR3004 SYNABS, PR1274/3-1, and PR1274/5-1, H.P.); and the Austrian Science Fund (FWF J4157-B30, M.R.). Parts of the work were funded by the European Union's Horizon 2020 research and innovation program through project RECOVER (GA101003589) to C.D.; the German Ministry of Research through the projects VARIPath (01KI2021) to V.M.C and NaFoUniMedCovid19–COVIM, FKZ: 01KX2021 to C.D. and V.M.C. This research used resources of the Advanced Light Source, which is a US Department of Energy (DOE) Office of Science User Facility under contract DE-AC02-05CH11231. Use of the SSRL, SLAC National Accelerator Laboratory, is supported by the DOE, Office of Science, Office of Basic Energy Sciences under contract DE-AC02–76SF00515. The SSRL Structural Molecular Biology Program is supported by the DOE Office of Biological and Environmental Research and by the National Institutes of Health, National Institute of General Medical Sciences (including P41GM103393). **Author contributions:** Conceptualization: S.M.R., M.Y., H.-C.K., V.M.C., H.P., I.A.W., and J.K. Patient recruitment and sample preparation: S.M.R., M.R., M.A.H., I.K., T.M.E., C.G., A.W., M.H., H.G., G.W., S.H., H.P., and J.K. Antibody production: S.M.R., S.v.H., E.S.-S., M.R., S.E.B., H.F.R., M.A.H., L.S., D.K., N.v.W., and J.K. Antibody reactivity testing: H.-C.K. Serological assays and neutralization testing: V.M.C., M.L.S., T.S., L.M.J., and C.D. Protein production and crystallography: M.Y., W.Y., Y.H., and H.T. Software: M.B., J.H., and S.M.R. Resources: V.M.C., M.H., G.W., D.S., C.D., H.P., and I.A.W. Writing, original draft: S.M.R., M.Y., H.-C.K., H.P., I.A.W., and J.K. Writing, review and editing: all authors. Supervision: S.M.R., M.Y., H.-C.K., V.M.C., H.P., I.A.W., and J.K. **Competing interests:** The German Center for Neurodegenerative Diseases (DZNE) and Charité-Universitätsmedizin Berlin have filed a patent application (application no. PCT/EP2021/064352) on antibodies for the treatment of SARS-CoV-2 infection described in an earlier publication, on which S.M.R., H.-C.K., V.M.C., E.S.-S., H.P., and J.K. are named as inventors. V.M.C. is named together with Euroimmun GmbH on a patent application filed recently regarding the diagnostic of SARS-CoV-2 by antibody testing. **Data and materials availability:** X-ray coordinates and structure factors are deposited at the RCSB Protein Data Bank under accession codes 7S5P, 7S5Q, and 7S5R. The amino acid sequences of the antibodies described in this study can be found in table S3. Nucleotide sequences have been deposited to GenBank (accession nos. OM457661 to OM457822). All requests for materials including antibodies, viruses, plasmids, and proteins generated in this study should be directed to the corresponding authors. Materials will be made available for noncommercial usage. This work is licensed under a Creative Commons Attribution 4.0 International (CC BY 4.0) license, which permits unrestricted use, distribution, and reproduction in any medium, provided the original work is properly cited. To view a copy of this license, visit https://creativecommons.org/licenses/by/4.0/. This license does not apply to figures/photos/artwork or other content included in the article that is credited to a third party; obtain authorization from the rights holder before using such material.

SUPPLEMENTARY MATERIALS

science.org/doi/10.1126/science.abm5835
Materials and Methods
Figs. S1 to S6
Tables S1 to S6
References (*32*–*45*)

View/request a protocol for this paper from *Bio-protocol*.

29 September 2021; accepted 18 January 2022
Published online 25 January 2022
10.1126/science.abm5835

Downloaded from https://www.science.org at Deutsches Zentrum fr Neurodegenerative Erkrankungen on June 14, 2022

Science

SARS-CoV-2 Beta variant infection elicits potent lineage-specific and cross-reactive antibodies

S. Momsen ReinckeMeng YuanHans-Christian KornauVictor M. CormanScott van HoofElisa Sánchez-SendinMelanie RambergerWenli YuYuanzi HuaHenry TienMarie Luisa SchmidtTatjana SchwarzLara Maria JeworowskiSarah E. BrandlHelle Foverskov RasmussenMarie A. HomeyerLaura StöfflerMartin BarnerDésirée KunkelShufan HuoJohannes HorlerNiels von WardenburgInge KroidlTabea M. EserAndreas WieserChristof GeldmacherMichael HoelscherHannes GänzerGünter WeissDietmar SchmitzChristian DrostenHarald PrüssIan A. WilsonJakob Kreye

Science, 375 (6582), • DOI: 10.1126/science.abm5835

Beta variant antibody responses

Several severe acute respiratory syndrome coronavirus 2 (SARS-CoV-2) variants of concern that either enhance infectivity or resist neutralization by sera from vaccinated or convalescent individuals have emerged. The variants Beta and Omicron in particular no longer bind many neutralizing antibodies that target the receptor-binding domain (RBD) of the SARS-CoV-2 spike protein. Reincke *et al*. isolated antibodies from Beta-infected patients and showed that although some bound both the Beta and the wild-type RBD, others were specific for Beta. Some of the Beta antibodies had genetic characteristics similar to wild-type antibodies that were sensitive to the Beta mutations. Whereas some antibodies appeared to use a noncanonical binding mode, others accommodated Beta mutations into known binding modes. This work provides insights for the design of next-generation vaccines and antibody therapeutics. —VV

View the article online
https://www.science.org/doi/10.1126/science.abm5835
Permissions
https://www.science.org/help/reprints-and-permissions

Downloaded from https://www.science.org at Deutsches Zentrum fr Neurodegenerative Erkrankungen on June 14, 2022

Use of this article is subject to the Terms of service

Science (ISSN) is published by the American Association for the Advancement of Science. 1200 New York Avenue NW, Washington, DC 20005. The title *Science* is a registered trademark of AAAS.
Copyright © 2022 The Authors, some rights reserved; exclusive licensee American Association for the Advancement of Science. No claim to original U.S. Government Works. Distributed under a Creative Commons Attribution License 4.0 (CC BY).